COMPUTER METHODS IN APPLIED MECHANICS AND ENGINEERING 38 (1983) 93–120
NORTH-HOLLAND PUBLISHING COMPANY

A FOUR-NODED THIN-PLATE BENDING ELEMENT USING SHEAR CONSTRAINTS—A MODIFIED VERSION OF LYONS' ELEMENT*

M.A. CRISFIELD
Transport and Road Research Laboratory, Crowthorne, Berkshire RG11 6AU, U.K.

Received 29 November 1982
Revised manuscript received 30 December 1982

Lyons [1] has presented a four-noded bending element that gives excellent numerical results and passes the patch test for a general quadrilateral. The element is derived, using the discrete-Kirchhoff method, with fifteen of the original twenty-seven displacement variables being eliminated via various constraints involving the shear strains. Some of these constraints are complicated involving, for example, an application of Green's theorem in applying a numerical integration around the boundary of the element, while two other constraints involve numerical integrations over the area of the element. Various matrix manipulations, including matrix division, are therefore required at the element level.

This paper presents a very similar element (the results appear to be identical for rectangles and parallelograms) which also passes the patch test for a general quadrilateral. However the constraints are now given, and derived, in explicit algebraic form. Fortran subroutines are provided for the major steps in the generation of the element stiffness matrix. The second part of the paper contains a comprehensive set of numerical examples in which the performance of the element is compared with that of two other elements; firstly, one of the best of the four-noded Mindlin elements (due to Hughes and Tezduyar) and secondly, the popular uniformly under-integrated serendipity Mindlin element.

1. Introduction

Although discrete-Kirchhoff elements [1–7] were introduced over ten years ago [2], they have not, with the possible exception of Irons' semi-loof shell element [4, 5], attained universal acceptance. Nonetheless, following a detailed comparison with other three-noded triangular elements, Batoz et al. [3] concluded that a discrete-Kirchhoff element was the best and, in particular, that it was better than a similar Mindlin [8] element which was derived using reduced integration [9, 10]. Following this observation, it would seem useful to conduct a similar experiment using four-noded quadrilaterals.

Such a four-noded discrete-Kirchhoff element has been presented by Lyons [1]. The quoted performance is excellent and, unlike many four-noded general quadrilaterals, the element passes the patch test [11]. However, in common with other discrete-Kirchhoff elements, it has not become popular. There would appear to be two reasons. Firstly, although the element has been mentioned in the books by Zienkiewicz [7] and Irons and Ahmad [5], details have so far only been published in Ph.D. thesis form [1]. Secondly, the derivation is both complex and cumbersome with numerical integration being required, not only for the integration of the

*The work described in this paper forms part of the programme of the Transport and Road Research Laboratory and is published by permission of the Director.

stiffness matrix, but also for the formation of the constraint matrix. (In the latter case, involving both area and boundary integrations.) Matrix manipulation, including matrix division, is also required before the constraint matrix is derived. Clearly such procedures are off-putting in comparison with the standard shape function approach of conventional (including Mindlin) displacement-based finite elements. It is perhaps pertinent, in relation to this observation, that two of the most popular discrete-Kirchhoff elements [4, 5, 11] have been described in books [5] and papers [11] with accompanying Fortran subroutines for the generation of the stiffness matrices.

In the theoretical part of the paper, an attempt is made to overcome some of these problems by devising an element, similar to Lyons', in which the constraints are derived in explicit algebraic form from the shape functions. Fortran subroutines are also provided. The approach is strongly influenced by the work of Tessler and Dong [12] on the application of shear constraints in relation to the analysis of a beam. Using such a technique, the constraints are not really 'discrete' but instead relate to complete 'shear strain modes'; hence, the absence of the terminology 'discrete-Kirchhoff' in the title of the present paper. The work is also strongly influenced by that of Hughes and Tezduyar [13] who use similar concepts to limit (but not, as at present, suppress) the shear deformations within a Mindlin plate element. This element is used in the second, numerical experimentation, part of the paper.

While comparisons could have been made with a number of four-noded elements [13–18], Hughes and Tezduyar's element has been chosen for the following reasons. It is not that difficult to code so that it could be used by the author to analyse a wide range of problems. It passes the patch test for a general quadrilateral (with imposed boundary displacements that are consistent with constant curvature and zero shear). It does not lock and possesses no spurious zero energy modes. It's numerical performance also appears to be very good and, in common with the present element, it uses uniform two-point Gaussian integration. In contrast with the present element, Hughes and Tezduyar's element can handle shear deformation as well as model thin plates.

Comparisons are also made with the popular eight-noded serendipity Mindlin element, which is uniformly under-integrated using two-point Gaussian integration [9, 10]. The main disadvantage of this element is that it 'locks' in very thin plate situations [16, 17]. While better displacement based Mindlin elements are available [19, 20], the use of the serendipity element serves to show that, for many problems, the four-noded elements surpass the performance of all but the best higher order elements.

2. Lyons' element

The genealogy of Lyons' element can be assumed to start with the Baldwin–Razzaque–Irons discrete-Kirchhoff element [6]. With this element, the serendipity shape functions are originally adopted for both the transverse displacement and the normal rotations. However, the resulting 24 (3×8) degrees-of-freedom are then reduced to 16 ($24 - 2 \times 4$) by forcing the shear strains to be zero at the four two-point Gauss stations (8 constraints). The element performs well but does not pass the patch test for a general quadrilateral. Irons [4, 5] took the next step by introducing a set of constraints in relation to his semi-loof shell element which, in plate terms, can be interpreted as follows.

(C1) The tangential shear strain shall be zero at the eight two-point Gauss stations of the *sides* of the element (8 constraints).

(C2) $\int \gamma_{xz} dA = \int \gamma_{yz} dA = 0$ (2 constraints) (1)
(see Fig. 1 for the adopted co-ordinate system).

(C3) $$\int \left(\frac{\partial \gamma_{xz}}{\partial x} + \frac{\partial \gamma_{yz}}{\partial y}\right) dA = 0 \quad \text{(1 constraint)}. \tag{2}$$

If this equation is multiplied by the shear modulus times the thickness it can be seen to give the equation for vertical equilibrium. Using Green's theorem it can be transposed to

$$\int \gamma_n ds = 0 \tag{3}$$

where γ_n is the shear strain normal to the boundary and the constraint involves an integration around the boundary of the element.

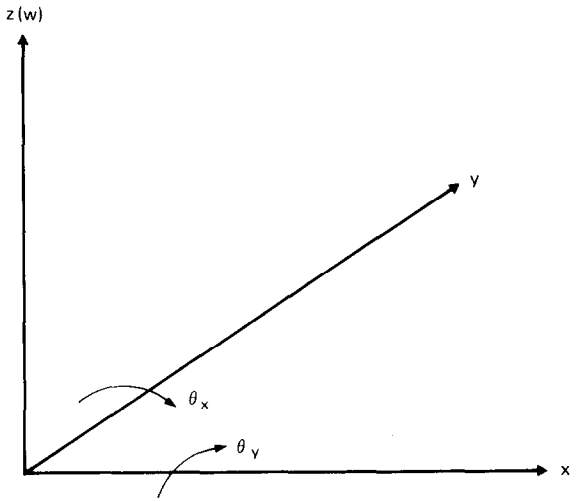

Fig. 1. Co-ordinates, w displacement and normal rotations.

Lyons [1] adopts these constraints for his ISOFLEX 8 element and uses two-point Gaussian integration to implement (1), while numerical integration, involving on this occasion the eight two-point Gauss points on the sides, is also used to implement (3). For his four-noded element, with which the present paper is concerned, Lyons adds the following constraint.

(C4) The rotations normal to the sides shall vary linearly along the sides (4 constraints).

In contrast to the Baldwin–Razzaque–Irons element which starts with the eight serendipity modes, Lyons' element originally adopts the nine Lagrangian shape functions ($27 = 3 \times 9$ degrees-of-freedom). To ease the later application of the constraints, these are expressed in hierarchical form, with

$$w = \sum_{i=1}^{4} H_i w_i + \sum_{i=5}^{9} H_i \Delta w_i, \tag{4}$$

$$\boldsymbol{\theta} = \sum_{i=1}^{4} H_i \boldsymbol{\theta}_i + \sum_{i=5}^{9} H_i \Delta \boldsymbol{\theta}_i \tag{5}$$

where $\boldsymbol{\theta}$ are the rotations of the normal, such that

$$\boldsymbol{\theta}^{\mathrm{t}} = \{\theta_x, \theta_y\} \tag{6}$$

and the sign convention is shown in Fig. 1. The full shape functions and derivatives are given in Appendix A. The summations $i = 5$–8 in (4) and (5) relate to the mid-side nodes and $i = 9$

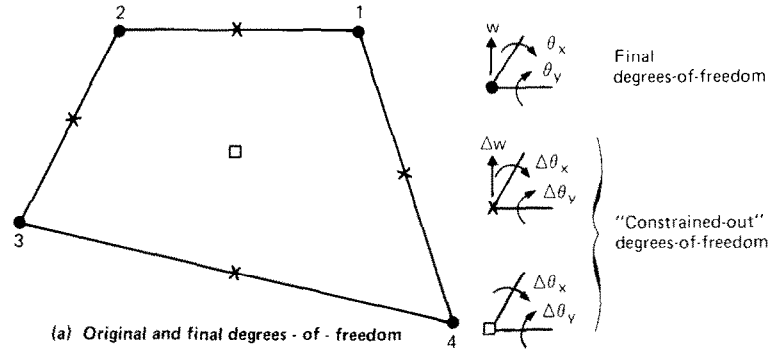

(a) Original and final degrees - of - freedom

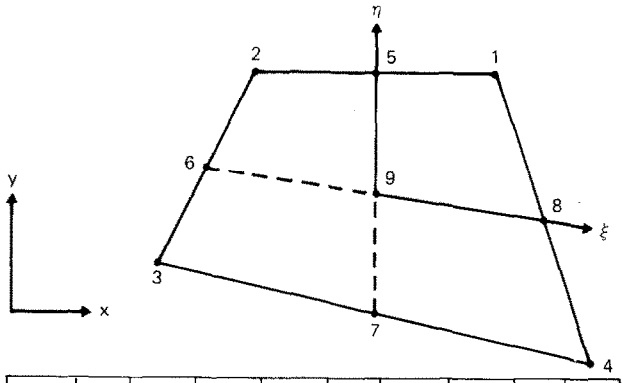

Node	1	2	3	4	5	6	7	8	9
ξ	1.0	−1.0	−1.0	1.0	0.0	−1.0	0.0	1.0	0.0
η	1.0	1.0	−1.0	−1.0	1.0	0.0	−1.0	0.0	0.0

(b) Node numbering and non-dimensional co-ordinates

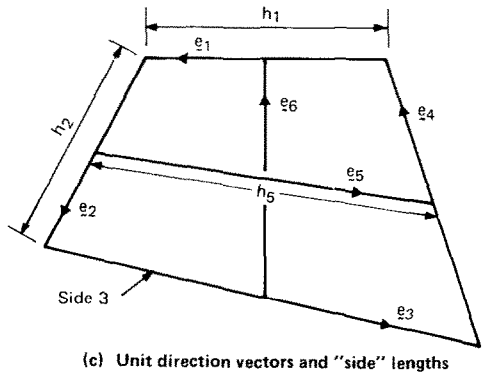

(c) Unit direction vectors and "side" lengths

Fig. 2. The plate element.

relates to the central node (Fig. 2(b)). Lyons' uses the fifteen constraints (C1)–(C4) to express Δw_{5-9} and $\Delta \boldsymbol{\theta}_{5-9}$ in terms of the other twelve basic variables w_{1-4} and $\boldsymbol{\theta}_{1-4}$. This is achieved by setting up a matrix equation of the form

$$\underset{15\times12}{\boldsymbol{M}_l}\ \boldsymbol{u}_l + \underset{15\times15}{\boldsymbol{M}_q}\ \Delta \boldsymbol{u}_q = \boldsymbol{0} \tag{7}$$

where $\boldsymbol{u}_l$ contains the basic (linear) displacements w_{1-4} and $\boldsymbol{\theta}_{1-4}$ while $\Delta \boldsymbol{u}_q$ contains the 'redundant' (quadratic) variables Δw_{5-9} and $\Delta \boldsymbol{\theta}_{5-9}$. The latter variables are then expressed in terms of $\boldsymbol{u}_l$ using

$$\Delta \boldsymbol{u}_q = -\boldsymbol{M}_q^{-1}\boldsymbol{M}_l\boldsymbol{u}_l = \boldsymbol{C}\boldsymbol{u}_l\,. \tag{8}$$

The objective of the theoretical part of the paper is to obtain explicit algebraic expressions in place of (8). (Not necessarily equivalent since different constraints are adopted.) With this in mind, it is useful to firstly study a beam so that the underlying concepts can be developed. This preliminary study is closely related to the work of Fraeijs de Veubeke [21] and Tessler and Dong [12].

3. Theory for a beam

Using Timoshenko's beam theory [22] the strain energy can be written as

$$\phi = \tfrac{1}{2}EI\int\left(\frac{\partial\theta}{\partial x}\right)^2 \mathrm{d}x + \tfrac{1}{2}G\bar{A}\int\gamma_x^2 \mathrm{d}x \tag{9}$$

where (Fig. 3)

$$\gamma_x = \theta + \partial w/\partial x \tag{10}$$

and θ is the rotation of the normal. If a single element is to be able to exactly represent a linearly varying bending moment, this normal rotation should be expressed as a quadratic in x. Hence, using the variables in Fig. 3,

$$\theta = \tfrac{1}{2}\begin{Bmatrix}1-\xi\\1+\xi\end{Bmatrix}^{\mathrm{t}}\begin{Bmatrix}\theta_1\\\theta_2\end{Bmatrix} + (1-\xi^2)\Delta\theta_q = \boldsymbol{H}_l^{\mathrm{t}}\boldsymbol{\theta}_l + H_q\Delta\theta_q \tag{11}$$

where, using the hierarchical concept, $\Delta\theta_q$ is the 'relative' rotation at 'q' ($\xi = 0$, Fig. 3), i.e. the full rotation at 'q' is $\frac{1}{2}(\theta_1+\theta_2)+\Delta\theta_q$.

If the element is to be able to simultaneously sustain no shear strain (i.e. satisfy the Kirchhoff mode), from (10), w should be a cubic in x, i.e.

$$w = \tfrac{1}{2}\begin{Bmatrix}1-\xi\\1+\xi\end{Bmatrix}^{\mathrm{t}}\begin{Bmatrix}w_1\\w_2\end{Bmatrix} + (1-\xi^2)\Delta w_q + [\tfrac{8}{3}\xi(1-\xi^2)\Delta w_c] = \boldsymbol{H}_l^{\mathrm{t}}w_l + H_q\Delta w_q + [H_c\Delta w_c]\,. \tag{12}$$

The terms in square brackets define a cubic mode that is superimposed on the linear and

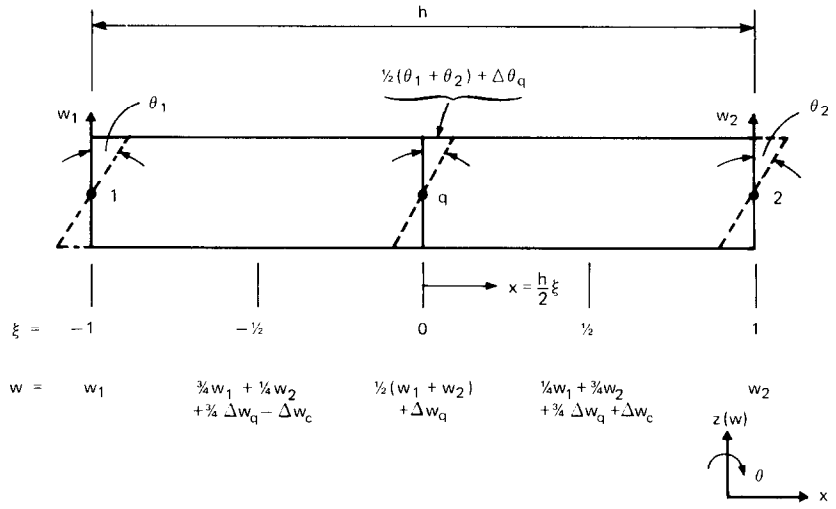

Fig. 3. The beam element.

quadratic terms. The square brackets are adopted since later work will investigate the effect of omitting this cubic term.

Using the displacement functions of (11) and (12), the shear strain (10) can be expressed as

$$\gamma_x = A_1 + A_2\xi + A_3\xi^2 \tag{13}$$

where

$$A_1 = \tfrac{1}{2}(\theta_1 + \theta_2) + (w_2 - w_1)/h + \Delta\theta_q + [16\Delta w_c/3h]\,, \tag{14}$$

$$A_2 = \tfrac{1}{2}(\theta_2 - \theta_1) - 4\Delta w_q/h\,, \tag{15}$$

$$A_3 = -\Delta\theta_q - [16\Delta w_c/h]\,. \tag{16}$$

Hence, if the shear strain is to be constrained to be zero, $A_1 = A_2 = A_3 = 0$ and

$$\Delta w_q = \tfrac{1}{8}h(\theta_2 - \theta_1)\,, \tag{17}$$

$$\Delta\theta_q = -\tfrac{3}{4}(\theta_1 + \theta_2) + \tfrac{3}{2}(w_1 - w_2)/h\,, \tag{18}$$

$$\Delta w_c = -\tfrac{1}{16}h\,\Delta\theta_q\,. \tag{19}$$

The constraints of (17)–(19) can now be used to eliminate Δw_q, $\Delta\theta_q$ and Δw_c so that, substituting into (11),

$$\theta = -\tfrac{1}{4}(\theta_1 + \theta_2) + \tfrac{3}{2}(w_1 - w_2)/h + \tfrac{1}{2}\xi(\theta_2 - \theta_1) + \xi^2(\tfrac{3}{4}(\theta_1 + \theta_2) - \tfrac{3}{2}(w_1 - w_2)/h)\,, \tag{20}$$

while, substituting into (12),

$$w = \tfrac{1}{2}\begin{Bmatrix}1-\xi\\1+\xi\end{Bmatrix}^{\mathrm{t}}\begin{Bmatrix}w_1\\w_2\end{Bmatrix} + \tfrac{1}{8}h(1-\xi^2)(\theta_2 - \theta_1) + [\xi(1-\xi^2)(\tfrac{1}{8}h(\theta_1 + \theta_2) - \tfrac{1}{4}(w_1 - w_2))] \tag{21}$$

Equation (21) (including the square bracketed term) is the standard cubic 'conforming shape function' that would be adopted for a conventional 'Kirchhoff energy approach', while (20) gives an expression for the normal rotation θ that is identical to the $-\partial w/\partial x$ term that would be obtained by differentiating (21). Therefore the formulation gives identical results to the conventional Kirchhoff energy approach and, since the γ_x^2 term is zero in (9), the shear strain energy may be omitted.

Consider now the effect of omitting the cubic Δw_c mode and modifying the constraints to relate to the two-point Gauss stations ($\xi = \pm\frac{1}{3}\sqrt{3}$), so that there is no shear strain at these points. This procedure ensures that the only remaining shear strain mode involves $(1-3\xi^2)$ which is, not only zero at the two-point Gauss stations, but also integrates to zero over the length of the element. Applying this technique and using (13)–(16)

$$A_2 = 0 \quad \Rightarrow \quad \text{equation (17)}, \tag{22}$$

while

$$A_1 + \tfrac{1}{3}A_3 = 0 \quad \Rightarrow \quad \text{equation (18)}. \tag{23}$$

Hence, substitution from (18) for $\Delta\theta_q$ into (11) for θ gives an identical expression (20) to that obtained previously. Also substituting (17) for Δw_q into (12) for w (with the square bracketed cubic term missing) gives (21) without the square bracketed term. Hence the stiffness matrix will be the same (when calculated from (9) without the shear energy). Also, a consistent constant line load vector, obtained from (21), will be unaffected by the presence, or otherwise, of the square bracketed cubic mode which integrates to zero. Similar methods will now be applied to the plate with a view to achieving, once more, shear strains that are 'effectively zero' so that the shear strain energy can be ignored.

4. Theory for a plate

Following the previous one-dimensional development, the strain energy will be expressed in the form

$$\phi = \int \boldsymbol{\chi}^{\mathrm{t}} \boldsymbol{D} \boldsymbol{\chi} \, \mathrm{d}A \tag{24}$$

where $\boldsymbol{\chi}$ is the 'strain' or 'curvature' vector

$$\boldsymbol{\chi}^{\mathrm{t}} = \left\{ \frac{\partial \theta_x}{\partial x}, \frac{\partial \theta_y}{\partial y}, \frac{\partial \theta_x}{\partial y} + \frac{\partial \theta_y}{\partial x} \right\} \tag{25}$$

and $\boldsymbol{D}$ is the 3×3 matrix of bending rigidities. (Note, with the above definition of $\boldsymbol{\chi}(3)$, $\boldsymbol{D}(3,3) = Et^3/24(1+\nu)$). The 'curvatures' $\boldsymbol{\chi}$ are related to the derivatives of the rotations functions (5) using

$$\begin{Bmatrix} \dfrac{\partial \theta_{x,y}}{\partial x} \\ \dfrac{\partial \theta_{x,y}}{\partial y} \end{Bmatrix} = [\boldsymbol{J}]^{-1} \begin{Bmatrix} \dfrac{\partial \theta_{x,y}}{\partial \xi} \\ \dfrac{\partial \theta_{x,y}}{\partial \eta} \end{Bmatrix} = [\boldsymbol{J}]^{-1} \begin{Bmatrix} \sum_{i=1}^{9} H_{\xi i}\, \theta_{xi,\,yi} \\ \sum_{i=1}^{9} H_{\eta i}\, \theta_{xi,\,yi} \end{Bmatrix} \tag{26}$$

where $\boldsymbol{J}^{-1}$ is the inverse Jacobian, and the convention $\theta_{x,y}$ means that either θ_x or θ_y is considered throughout the equation. The terms $H_{\xi i}$ and $H_{\eta i}$ are the derivatives of the shape functions with respect to ξ and η, respectively (see Appendix A). Using (26), the 'curvatures' can easily be expressed in terms of the original 27 (3×9) degrees-of-freedom by simply clearing the required connection matrix $\boldsymbol{B}$ and then inserting the terms from (26) into their appropriate positions. This 'curvature'–nodal displacement matrix is next condensed to a 3×12 matrix, $\boldsymbol{B}_c$ which involves only the corner node variables, $\boldsymbol{u}_l$, i.e.

$$\underset{3\times 27}{\boldsymbol{\chi}} = \underset{3\times 27}{\boldsymbol{B}}\ \boldsymbol{u} = \begin{bmatrix} \underset{3\times 12}{\boldsymbol{B}_l} & \underset{3\times 15}{\boldsymbol{B}_q} \end{bmatrix} \begin{Bmatrix} \boldsymbol{u}_l \\ \Delta \boldsymbol{u}_q \end{Bmatrix} = \underset{3\times 12}{\boldsymbol{B}_c}\ \boldsymbol{u}_l \,. \tag{27}$$

The constrained matrix $\boldsymbol{B}_c$ is (conceptually) derived from the full matrix $\boldsymbol{B}$ using the partitioning of (27) and a constraint relationship of the form of (8), i.e.

$$\underset{3\times 12}{\boldsymbol{B}_c} = \underset{3\times 12}{\boldsymbol{B}_l} + \underset{3\times 15}{\boldsymbol{B}_q}\ \underset{15\times 12}{\boldsymbol{C}} \,. \tag{28}$$

The stiffness matrix then follows in the standard manner via

$$\underset{12\times 12}{\boldsymbol{K}} = \int \boldsymbol{B}_c^{\mathrm{t}} \boldsymbol{D} \boldsymbol{B}_c \mathrm{d}A \,. \tag{29}$$

Equations (27) and (28) have followed Lyons and have adopted Lagrangian functions for both $\boldsymbol{\theta}$ and w so that fifteen 'redundant' variables have been constrained out. However, it will be shown that the w_q term is unnecessary and that serendipity functions could have originally been adopted for w.

Before considering, in detail, the derivation of the constraints, it is useful to generate a set of unit direction vectors $\boldsymbol{e}_1$–$\boldsymbol{e}_6$ for the element (see Fig. 2(c)). These vectors relate to the four sides 1–4 and the centre-lines 5 and 6 (collectively referred to, in future, as the 'sides'). The 'side' lengths, h_1–h_6 (Fig. 2(c)) are also required and for $i = 1$–4

$$\boldsymbol{e}_i(1) = (x_{i+} - x_i)/h_i, \qquad \boldsymbol{e}_i(2) = (y_{i+} - y_i)/h_i \tag{30}$$

where, throughout the paper $i+$ ($i = 1$–4) refers to the node anti-clockwise ahead of node i, i.e. (see Fig. 2(a))

$$\text{for } i = 1\text{–}4 \quad i+ = 2, 3, 4, 1 \,. \tag{31}$$

The centre-line vectors $\boldsymbol{e}_5$ and $\boldsymbol{e}_6$ and lengths h_5 and h_6 are computed in a similar manner.

Consider now, for example, side 3 (Fig. 2(c)) and, using the beam approach of (13)–(16) for guidance, it can be seen that the tangential shear strain component $\gamma_{t,3}$ can be expressed as

$$\gamma_{t,3} = \tfrac{1}{2}\boldsymbol{e}_3^t(\boldsymbol{\theta}_3 + \boldsymbol{\theta}_4) + \tfrac{1}{2}\xi\boldsymbol{e}_3^t(\boldsymbol{\theta}_4 - \boldsymbol{\theta}_3) + (1-\xi^2)\boldsymbol{e}_3^t\Delta\boldsymbol{\theta}_7 + (w_4 - w_3)/h_3 - 4\xi\Delta w_7/h_3 . \tag{32}$$

Again following the beam approach, it is required that the coefficient of the linear ξ term should be zero (see (22)) and that the constant term plus one-third of the coefficient of the quadratic ξ^2 term should also be zero (see (23)), i.e.

$$\Delta w_7 = -\tfrac{1}{8}h_3\boldsymbol{e}_3^t(\boldsymbol{\theta}_3 - \boldsymbol{\theta}_4) \tag{33}$$

and

$$\boldsymbol{e}_3^t\Delta\boldsymbol{\theta}_7 = -\tfrac{3}{4}\boldsymbol{e}_3^t(\boldsymbol{\theta}_3 + \boldsymbol{\theta}_4) + \tfrac{3}{2}(w_3 - w_4)/h_3 . \tag{34}$$

Equations (33) and (34) are equivalent to (17) and (18) for the beam and relate to the constraint (C1). Consider now the other constraint (C4) that Lyons applies on a side. This constraint forces the normal rotation to vary linearly along the side so that, still considering side 3, $\Delta\theta_{7n} = 0$ (Fig. 2(b)). This condition is given by

$$\boldsymbol{n}_3^t\Delta\boldsymbol{\theta}_7 = 0 \tag{35}$$

where $\boldsymbol{n}_3$ is the unit normal vector on side 3 which is related to the computed unit side vector $\boldsymbol{e}_3$ via

$$\boldsymbol{n}_3(1) = -\boldsymbol{e}_3(2), \qquad \boldsymbol{n}_3(2) = \boldsymbol{e}_3(1) . \tag{36}$$

Combining (34) and (35) and solving for $\Delta\boldsymbol{\theta}_7$

$$\Delta\boldsymbol{\theta}_7 = (-\tfrac{3}{4}\boldsymbol{e}_3^t(\boldsymbol{\theta}_3 + \boldsymbol{\theta}_4) + \tfrac{3}{2}(w_3 - w_4)/h_3)\boldsymbol{e}_3 . \tag{37}$$

The final constraints for side 3 are therefore expressed by (33) and (37). These constraints can be generalised to relate to all four sides so that, for $i = 1$–4

$$\Delta\boldsymbol{\delta}_{i+4} = \boldsymbol{C}_{a,i}\boldsymbol{\delta}_i + \boldsymbol{C}_{b,i}\boldsymbol{\delta}_{i+} \tag{38}$$

where

$$\boldsymbol{\delta}_i^t = \{w_i, \theta_{xi}, \theta_{yi}\}, \qquad \boldsymbol{\delta}_{i+}^t = \{w_{i+}, \theta_{xi+}, \theta_{yi+}\}, \qquad \Delta\boldsymbol{\delta}_i^t = \{\Delta w_i, \Delta\theta_{xi}, \Delta\theta_{yi}\} \tag{39}$$

and the constraint matrices $\boldsymbol{C}_{a,i}$ and $\boldsymbol{C}_{b,i}$ are given by

$$\boldsymbol{C}_{a,i} = \begin{bmatrix} 0 & -\frac{1}{8}h_i\boldsymbol{e}_i(1) & -\frac{1}{8}h_i\boldsymbol{e}_i(2) \\ \frac{3}{2}\boldsymbol{e}_i(1)/h_i & -\frac{3}{4}\boldsymbol{e}_i(1)\boldsymbol{e}_i(1) & -\frac{3}{4}\boldsymbol{e}_i(1)\boldsymbol{e}_i(2) \\ \frac{3}{2}\boldsymbol{e}_i(2)/h_i & -\frac{3}{4}\boldsymbol{e}_i(1)\boldsymbol{e}_i(2) & -\frac{3}{4}\boldsymbol{e}_i(2)\boldsymbol{e}_i(2) \end{bmatrix},$$

$$\boldsymbol{C}_{b,i} = \begin{bmatrix} 0 & \frac{1}{8}h_i\boldsymbol{e}_i(1) & \frac{1}{8}h_i\boldsymbol{e}_i(2) \\ -\frac{3}{2}\boldsymbol{e}_i(1)/h_i & -\frac{3}{4}\boldsymbol{e}_i(1)\boldsymbol{e}_i(1) & -\frac{3}{4}\boldsymbol{e}_i(1)\boldsymbol{e}_i(2) \\ -\frac{3}{2}\boldsymbol{e}_i(2)/h_i & -\frac{3}{4}\boldsymbol{e}_i(1)\boldsymbol{e}_i(2) & -\frac{3}{4}\boldsymbol{e}_i(2)\boldsymbol{e}_i(2) \end{bmatrix} \tag{40}$$

where the rotational convention of (31) is used to define the node $i+$.

The most difficult constraints involve the central bubble functions (the H_9 modes in Appendix A). Here, we part company from Lyons, and consider the variation of tangential shear strain along the centre-lines 5 and 6 (Fig. 2(c)). Using the shape functions of (4) and (5), with details from Appendix A, the tangential shear strain along 'side' 5 (the centre-line $\eta = 0$, Fig. 2(b)), can be expressed as

$$\gamma_{t,5} = \tfrac{1}{4}\sum_{i=1}^{4}(1+\xi_i\xi)\boldsymbol{e}_5^t\boldsymbol{\theta}_i + \tfrac{1}{2}\sum_{i=5}^{8}(1-\eta_i^2\xi)(1+\xi_i\xi)\boldsymbol{e}_5^t\Delta\boldsymbol{\theta}_i + \frac{1}{2h_5}\sum_{i=1}^{4}\xi_i w_i + \frac{2}{h_5}\sum_{i=5}^{8}(-\eta_i^2\xi+\tfrac{1}{2}\xi_i)\Delta w_i - \frac{4\xi}{h_5}\Delta w_9 + (1-\xi^2)\boldsymbol{e}_5^t\Delta\boldsymbol{\theta}_9\,. \tag{41}$$

Following the beam approach, one of the conditions for enforcing 'effectively zero tangential shear strain' along this line is that the constant term plus one-third of the coefficient of the quadratic ξ^2 term should be zero (see (23)). This condition gives

$$\boldsymbol{e}_5^t\Delta\boldsymbol{\theta}_9 = -\tfrac{3}{8}\sum_{i=1}^{4}\boldsymbol{e}_5^t\boldsymbol{\theta}_i - \tfrac{3}{4}\sum_{i=5}^{8}(1-3\eta_i^2)\boldsymbol{e}_5^t\Delta\boldsymbol{\theta}_i - \frac{3}{4h_5}\sum_{i=1}^{4}\xi_i w_i - \frac{3}{2h_5}\sum_{i=5}^{8}\xi_i\Delta w_i \tag{42}$$

while the equivalent condition for 'side' 6 is

$$\boldsymbol{e}_6^t\Delta\boldsymbol{\theta}_9 = -\tfrac{3}{8}\sum_{i=1}^{4}\boldsymbol{e}_6^t\boldsymbol{\theta}_i - \tfrac{3}{4}\sum_{i=5}^{8}(1-3\xi_i^2)\boldsymbol{e}_6^t\Delta\boldsymbol{\theta}_i - \frac{3}{4h_6}\sum_{i=1}^{4}\eta_i w_i - \frac{3}{2h_6}\sum_{i=5}^{8}\eta_i\Delta w_i\,. \tag{43}$$

At this stage, one might consider the other 'beam condition' for enforcing 'effectively zero tangential shear strain'. This condition requires that the coefficient of ξ in (41) should be zero (see (22)) and would lead to

$$\Delta w_9 = \tfrac{1}{16}h_5\sum_{i=1}^{4}\xi_i\boldsymbol{e}_5^t\boldsymbol{\theta}_i + \tfrac{1}{8}h_5\sum_{i=5}^{8}\xi_i\boldsymbol{e}_5^t\Delta\boldsymbol{\theta}_i - \tfrac{1}{2}\sum_{i=5}^{8}\eta_i^2\Delta w_i\,. \tag{44}$$

The problem then arises that a similar constraint along 'side' 6 ($\xi = 0$) would lead to a different term for Δw_9. This issue is confronted, and overcome, in [20] which describes a constrained Mindlin element that allows for shear deformation. However the problem can be simply avoided here by noting that, with the present thin plate formulation, there is no need to define a constant for Δw_9 since it does not feature in the bending strain energy and the shear strain energy is neglected, as being approximately zero. To appreciate that Δw_9 does not feature in the bending strain energy, one may observe from (24)–(27), that the original $\boldsymbol{B}$ matrix only involves $\boldsymbol{\theta}_{1\text{–}4}$ and $\Delta\boldsymbol{\theta}_{5\text{–}9}$. Also the constraints to eliminate $\Delta\boldsymbol{\theta}_9$ (see (42) and (43)), although they introduce $w_{1\text{–}4}$ and $\Delta w_{5\text{–}8}$, do not include Δw_9; nor do the side constraints for $\Delta\boldsymbol{\delta}_{5\text{–}8}$ ((38) and (39)).

To complete the algebraic expressions for the constraints, (42) and (43) must be combined and solved for $\Delta\boldsymbol{\theta}_9$. To this end, it is useful to generate the unit normal vectors $\boldsymbol{n}_5$ and $\boldsymbol{n}_6$ (from the computed $\boldsymbol{e}_5$ and $\boldsymbol{e}_6$) using

$$\boldsymbol{n}_5^t = \{-\boldsymbol{e}_5(2),\ \boldsymbol{e}_5(1)\}, \qquad \boldsymbol{n}_6^t = \{-\boldsymbol{e}_6(2),\ \boldsymbol{e}_6(1)\} \tag{45}$$

so that

$$\boldsymbol{e}_5^{\mathrm{t}}\boldsymbol{n}_5 = \boldsymbol{e}_6^{\mathrm{t}}\boldsymbol{n}_6 = 0\,. \tag{46}$$

The following scalar is also required

$$\phi = \boldsymbol{e}_5(1)\boldsymbol{e}_6(2) - \boldsymbol{e}_5(2)\boldsymbol{e}_6(1)\,. \tag{47}$$

Using these terms, (42) and (43) can be solved to give

$$\Delta\boldsymbol{\theta}_9 = -\tfrac{3}{8}\sum_{i=1}^{4}\boldsymbol{\theta}_i - \tfrac{3}{4}\sum_{i=5}^{8}\left[[\boldsymbol{I}] - \frac{\xi_i^2}{3\phi}[\boldsymbol{n}_5\boldsymbol{e}_6^{\mathrm{t}}] + \frac{\eta_i^2}{3\phi}[\boldsymbol{n}_6\boldsymbol{e}_5^{\mathrm{t}}]\right]\Delta\boldsymbol{\theta}_i$$
$$-\frac{3}{4\phi}\sum_{i=1}^{4}\left(\frac{\eta_i}{h_6}\boldsymbol{n}_5 - \frac{\xi_i}{h_5}\boldsymbol{n}_6\right)w_i - \frac{3}{2\phi}\sum_{i=5}^{8}\left(\frac{\eta_i}{h_6}\boldsymbol{n}_5 - \frac{\xi_i}{h_5}\boldsymbol{n}_6\right)\Delta w_i\,. \tag{48}$$

Equations (38) and (48) define the complete system of constraints. Before describing the formation of the stiffness matrix, the ordering of the variables needs to be defined. To this end, let the final variables $\boldsymbol{u}_l$ (see (27)) be defined by

$$\boldsymbol{u}_l^{\mathrm{t}} = \{\boldsymbol{\delta}_1^{\mathrm{t}}, \boldsymbol{\delta}_2^{\mathrm{t}}, \boldsymbol{\delta}_3^{\mathrm{t}}, \boldsymbol{\delta}_4^{\mathrm{t}}\} \tag{49}$$

where, for $i = 1$–4, $\boldsymbol{\delta}_i$ have been defined in (39). The 'redundant' quadratic variables $\Delta\boldsymbol{u}_{\mathrm{q}}^{\mathrm{t}}$ (see (27)) will be defined by

$$\Delta\boldsymbol{u}_{\mathrm{q}}^{\mathrm{t}} = \{\Delta\boldsymbol{\delta}_5^{\mathrm{t}}, \Delta\boldsymbol{\delta}_6^{\mathrm{t}}, \Delta\boldsymbol{\delta}_7^{\mathrm{t}}, \Delta\boldsymbol{\delta}_8^{\mathrm{t}}, \Delta\boldsymbol{\delta}_9^{\mathrm{t}}\} \tag{50}$$

where, for $i = 5$–9, $\Delta\boldsymbol{\delta}_i$ have also been defined in (39) although it should be noted that Δw_9 is set to zero.

The stiffness matrix is formed in the following manner (Steps 4–7 are contained in two Fortran subroutines given in Appendix B).

Step 1. Apply the preliminary geometry calculations to obtain $\boldsymbol{e}_1$–$\boldsymbol{e}_6$ and h_1–h_6 (see (30) and Fig. 2(c)).

Step 2. Apply two-by-two Gaussian integration and loop through the four Gauss points.

For each Gauss point, apply steps (3)–(8).

Step 3. Calculate the Jacobian, $\boldsymbol{J}$ and the inverse Jacobian, $\boldsymbol{J}^{-1}$, in the standard manner.

Step 4. Use the shape function derivatives $H_{\xi i}$, $H_{\eta i}$ for $i = 1$–9 (see Appendix A) to form the full unconstrained $\boldsymbol{B}$ matrix (see (26) and (27)).

Step 5. Use (45)–(48) to derive a 2×24 constraint matrix $\boldsymbol{C}_9$ to express $\Delta\boldsymbol{\theta}_9$ in terms of the remaining variables (see subroutine 'BUBCON', Appendix B).

Step 6. Pre-multiply this matrix by the 2×2 $\Delta\boldsymbol{\theta}_9$ terms in the $\boldsymbol{B}$ matrix and add the resulting matrix into the first 24 (3×8) columns of the original $\boldsymbol{B}$ matrix.

Step 7. Apply the constraints of (38) to the mid-side terms in the $\boldsymbol{B}$ matrix (columns 13–24) and add the resulting terms into the first 12 columns. These first 12 columns now represent the required constrained 'curvature'-displacement matrix, $\boldsymbol{B}_{\mathrm{c}}$ (see (27)).

Step 8. Add in the Gauss point contribution to the integrated stiffness matrix $\boldsymbol{K}$ (see (29)).

Steps 4–7 involve the important generation of the constrained $\boldsymbol{B}_c$ matrix (27) and a Fortran subroutine for this purpose (subroutine BMATRIX) is given in Appendix B.

Since the Δw_9 term is not required for the stiffness matrix, it will also be neglected for the generation of a 'consistent' uniformly distributed load vector (which is not fully consistent). To this end, (4) is combined with the generalised version of (33) (the first row of (38)) which, for $i = 1$–4 gives

$$\Delta w_{i+4} = -\tfrac{1}{8} h_i \boldsymbol{e}_i^{\mathrm{t}} (\boldsymbol{\theta}_i - \boldsymbol{\theta}_{i+}) \,. \tag{51}$$

The Δw_9 variable is set to zero. In [20] an expression is obtained for Δw_9 (using an equation related to (44)) and the bubble function term is included in the generation of the uniformly distributed load vector. Except for very coarse meshes, when somewhat more flexible responses were achieved, the introduction of this term had a negligible effect on the solution.

5. Hughes and Tezduyar's element

Since this element [13] will feature in the numerical comparisons, the main characteristics will be briefly described. The element is based upon Mindlin theory so that not only the bending energy is included (equation (24)), but also the shear energy (as in the equivalent beam formulation of (9). The stiffness matrix, associated with the bending energy, is standard and involves bi-linear expressions (H_i, $i = 1$–4 in Appendix A) for the normal rotations, $\boldsymbol{\theta}$. However, the shear stiffness terms differ from those that would be derived from the standard addition of bi-linear functions for the transverse displacement w. The differences follow from the *conceptual* use of serendipity (H_i, $i = 1$–8 in Appendix A) expressions for w. The extra Δw_{5-8} terms are then (conceptually) eliminated by forcing the tangential shear strains to be constant on the sides. However the final formulation does not conform fully with the resulting shape functions. Instead, the shape functions are used to generate the shear strains at the corners, but then, a bi-linear variation of shear strain is forced to pass through these values at the corners. It is not entirely clear what affect these modifications have on the transverse displacement, w, so that, as with the present thin plate element, there are difficulties with the definition of a 'consistent' uniformly distributed load vector. Hughes and Tezduyar [13] use a 'lumped load' matrix which effectively only employs the shape functions H_{1-4}. However, since the constraint of (51) is adopted in the build-up of the element, it could be argued that H_{5-8} should also be employed, with (51) being used to define Δw_{5-8}. This procedure is identical to that already described for the proposed thin-plate element. Both 'lumped load' vectors and this 'more consistent' uniformly distributed load vector will be used in the following numerical experiments.

6. Numerical experiments

All of the calculations were performed on the Transport and Road Research Laboratory Cyber 170-720 using single precision 60 bit words. Unless it is stated otherwise, the length L was set to 10.0, the thickness t to 0.1, Young's modulus E to 1000 and Poisson's ratio to 0.3.

Much of the nomenclature follows that adopted by Hughes et al. [13, 16, 19]. For instance two types of simply supported boundary conditions are used: SS_1 in which only the transverse displacement w is set to zero and SS_2 in which both w and the tangential rotation are restrained to zero. The abbreviation CL implies a fully clamped boundary while the loading is specified by U for a uniformly distributed load or C for a central point load. N_{el} refers to the number of elements used to idealise the structure and usually relates to a symmetric quarter of the plate.

The following notation is used to classify the different elements and loading approximations.

- T the present thin-plate element,
- TP the present thin-plate element with 'lumped point loads' to simulate the uniformly distributed loading,
- TC the present thin-plate element with 'consistent' (as previously defined) loading for the uniformly distributed loads,
- M Hughes and Tezduyar's Mindlin element [13],
- MP Hughes and Tezduyar's element with 'lumped point loads' to simulate the uniformly distributed loading,
- MC Hughes and Tezduyar's element with 'consistent' (as previously defined) loading for the uniformly distributed loads,
- S8 the standard eight-noded serendipity Mindlin element with uniform two-point Gaussian integration [9, 10]. 'Consistent' load vectors are used for any uniformly distributed loading.

Where, with a uniformly distributed loading, the results for TP and TC coincide, the adopted nomenclature will be simply truncated to T. A similar convention will be applied to the four-noded Mindlin element.

Before comparing the responses of the different elements, it is worth emphasising that the four-noded elements T and M pass the patch test as general quadrilaterals (with prescribed boundary displacements that are consistent with constant curvature and zero shear strain) while the eight-noded element S8 only passes this test for rectangles and parallelograms. All three elements give excellent results for Robinson's 'single element test' [23]. It should be noted that the results for Hughes and Tezduyar's Mindlin element M have not been taken from [13] but are rather from the author's programming of that element. The results do, however, coincide with those of [13] (the MP results for uniformly distributed loads) for those examples also considered in that publication.

(a) *Square plates.* For these much quoted examples, N_{el} refers to the number of uniform square elements within a symmetric quarter. The result are compared in Figs. 4 and 5, with the bending moments of Fig. 5 being taken from the two-point Gaussian integration station nearest the centre of the plate. The results, obtained for the thin plate element T (with TC for example SS_2–U), were found to be identical to those given by Lyons [1] for his four-noded ISOFLEX 4 element. On average, these results are better than those given by the other two (M and S8) elements. For this conclusion to be valid, the 'consistent' load vector must be applied with the T element for the SS_2–U example. In contrast, more accurate (stiffer solutions are obtained for the four-noded Mindlin element M, when 'lumped point loads' are used. Both four-noded elements give better convergence characteristics for the central displacement, than

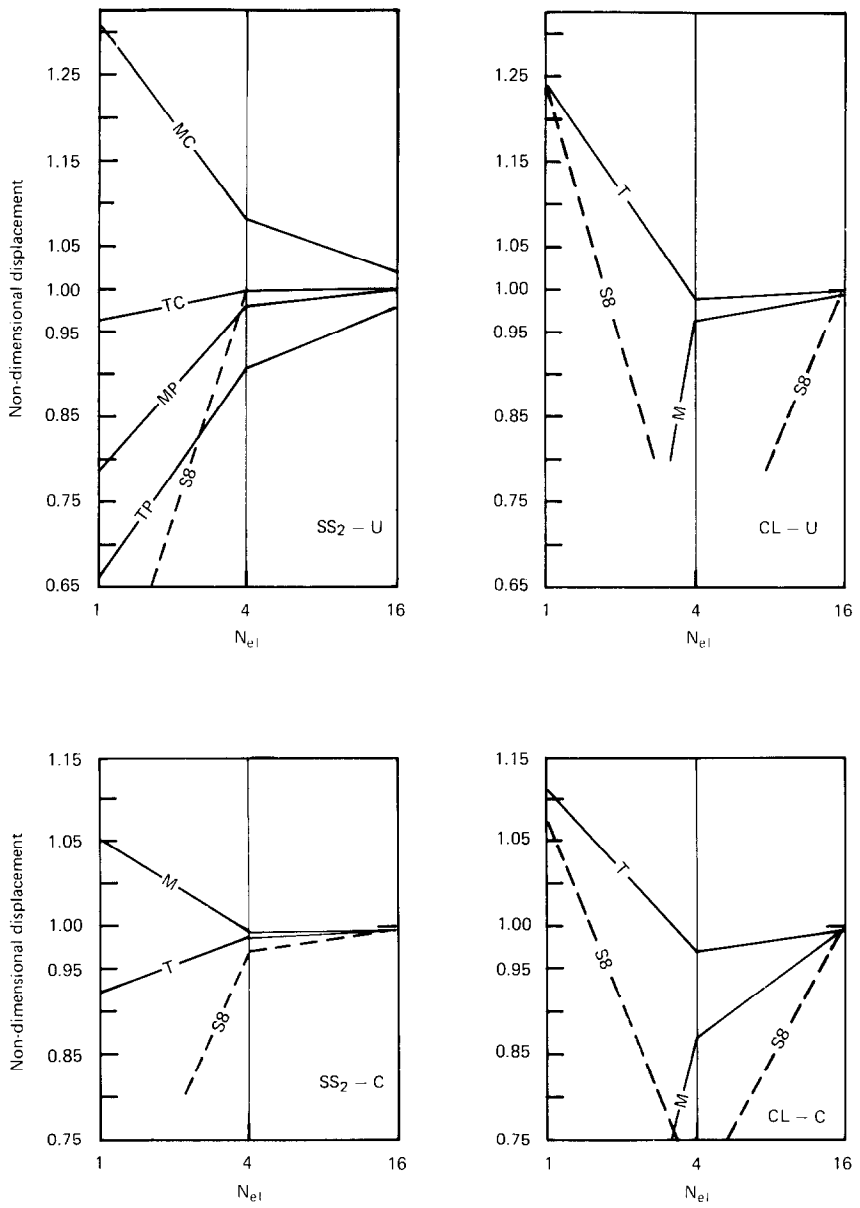

Fig. 4. Convergence characteristics for thin square plates: central deflection normalised with respect to 'exact' thin plate theory [23].

the eight-noded element S8. However, the four-noded Mindlin element, M does have a draw-back which is illustrated in Fig. 6, which plots the bending moments across the centre-line of the simply supported plate subject to a central point load (SS_2–C). The finite element results are taken directly from the row of two-point Gauss stations nearest to the centre-line (see Fig. 6) and the oscillatory nature of the moments, given by the Mindlin element M, can be clearly seen. The moments given by this element are far more accurate at

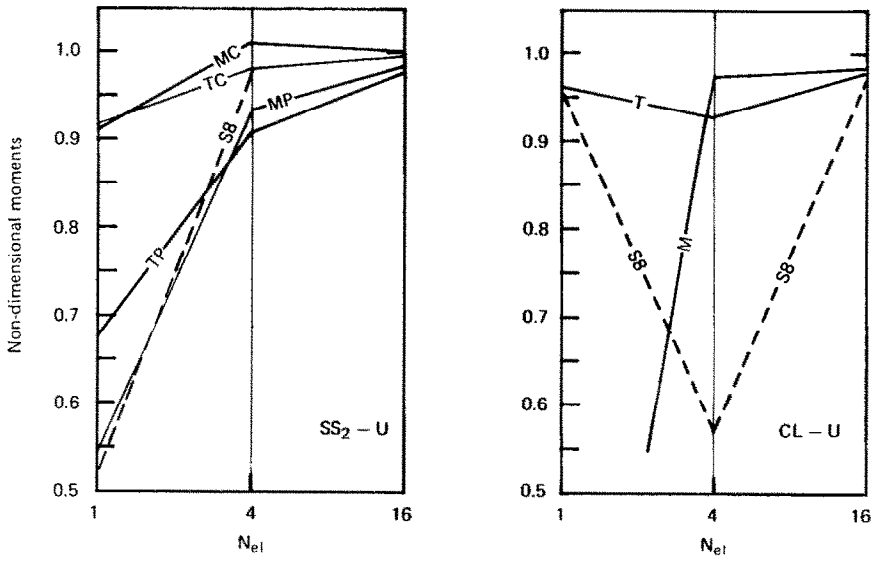

Fig. 5. Convergence characteristics for thin square plates: bending moment at Gauss point nearest centre, normalised with respect to 'exact' moment of thin plate theory [23].

its centroid. However, it would seem to be a disadvantage, particularly for problems involving plasticity, to have accurate 'stresses' at points which differ from those used for the basic numerical integration process (in this case, the two-point Gauss stations). In contrast, with the T and S8 elements, an efficient local (at the element level) smoothing [25] can be used to derive a reasonably accurate overall stress pattern.

(b) *Rectangular plates.* Robinson has argued [15] that the square plate does not adequately measure the response of an element and that rectangular plates, with different aspect ratios, should be used. The results of such a study are plotted in Figs. 7 and 8. (With $L = 10$ being maintained as the shorter length and uniform meshes being used to idealise a quarter of each plate.) Again, the present thin-plate element T gives excellent results (with the consistent load vectors for uniformly distributed loads), which are superior to those given by the two Mindlin elements.

(c) *Circular plate.* The geometry and mesh divisions for the eight-noded S8 element are given Fig. 9. The adopted idealisation is identical for the four-noded elements with the exception that straight lines are drawn between the corner nodes. This geometric idealisation is not necessarily the best that can be achieved with straight-sided elements, since only the corner nodes are on the true boundary, while it would be possible to adopt 'best-fit' straight-lines to the perimeter. However the adopted procedure is simple and allows some comparison to be made between the different elements (Fig. 10), although it will tend to lead to over-stiff solutions for coarse meshes.

The expected advantages (on an element-for-element basis) of the higher order S8 element are realised for these examples (Fig. 10), which involve curved boundaries. However, the results given by the four-noded elements are very reasonable, considering they have straight sides. With the exception of the CL–U example, the solutions given by the present thin-plate element T are as good, or better, than those given by the Mindlin element M.

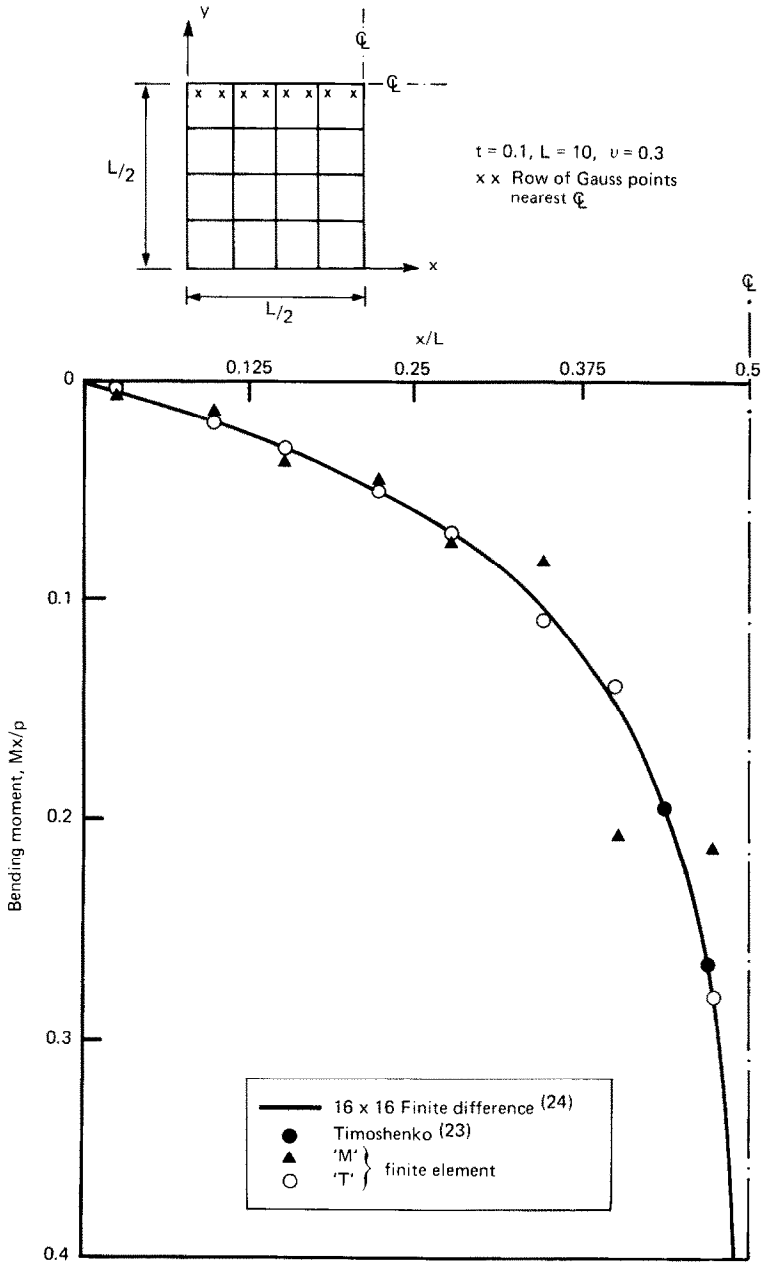

Fig. 6. Distribution of bending moments across the centre-line of a simply supported plate subject to a central point load (SS_2–C).

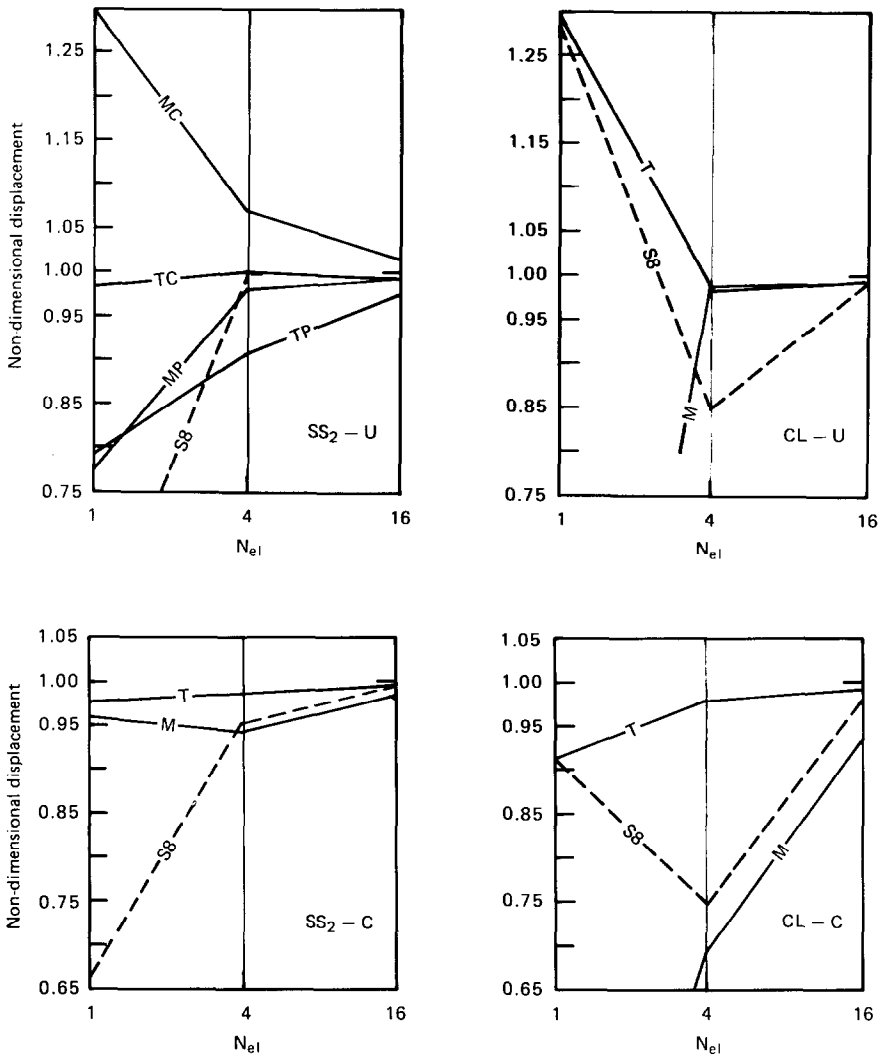

Fig. 7. Convergence characteristics for thin rectangular plates ($B/L = 2.0$): central deflection normalised with respect to exact thin plate theory [23].

(d) *A skew-plate, simply supported on two sides.* Razzaque [26] has used the Razzaque–Allman triangle [26, 27] to analyse the skew plate, of Fig. 11, subject to a uniformly distributed load. This plate has 'bridge type' boundary conditions, being simply supported on two opposite sides. Razzaque also gives [26] a 16×16 finite difference solution (central deflection of $0.007945qL^4/D$ and central bending moment M_y of $0.09589qL^2$), which has been used here as the yardstick. The results, which are plotted in Figs. 12 and 13, relate to two different boundary conditions on the simply supported edges: SS_1 with just w and SS_2 with both w and θ_x set to zero. Razzaque only gives one set of results, since it is not entirely clear to which boundary conditions they apply, they have been plotted on both the SS_1 and SS_2 figures. (The difference, between the two approaches, are very small for the T, M and S8 elements.) Razzaque's idealisations actually used twice the number elements indicated in Figs. 12 and 13

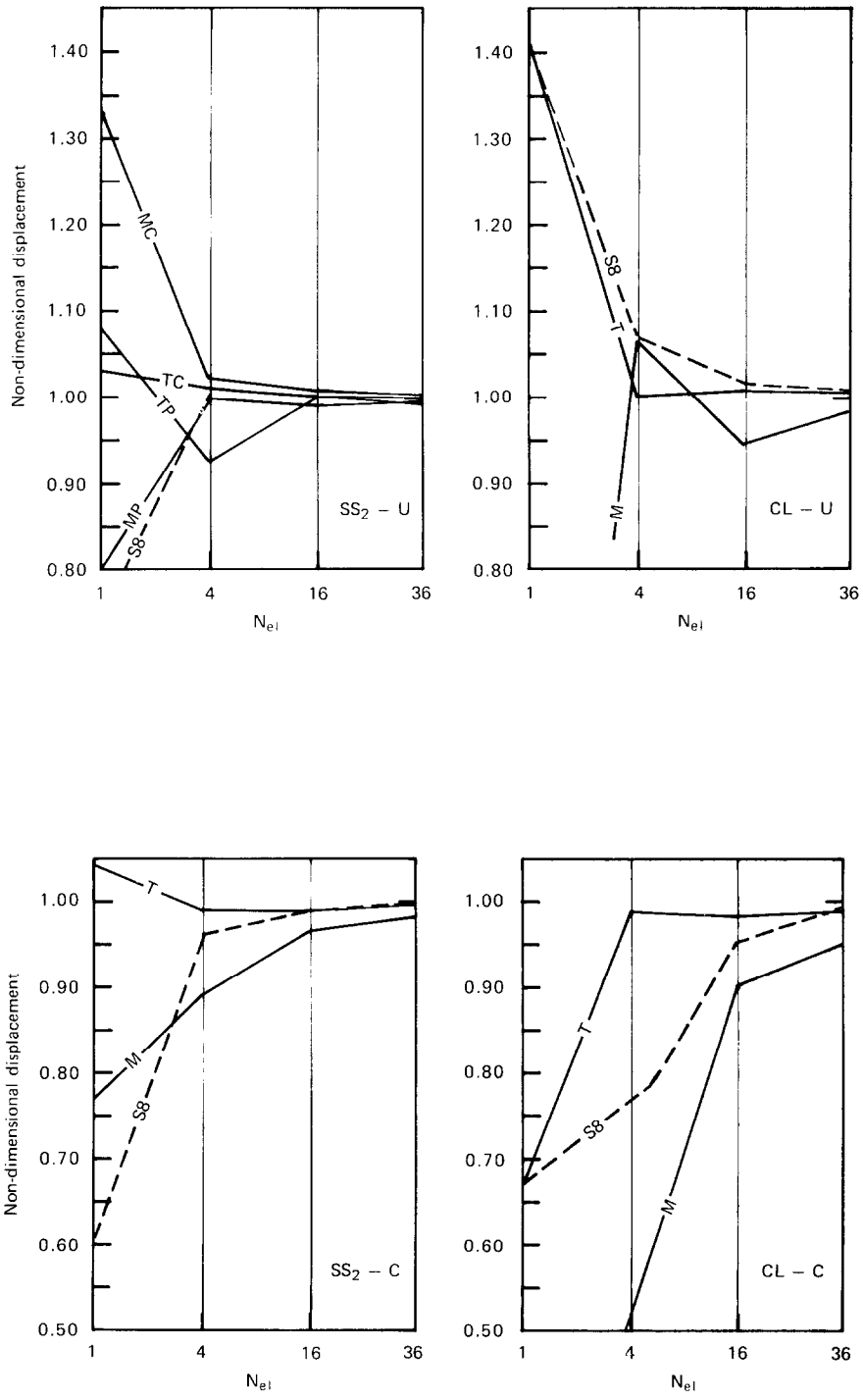

Fig. 8. Convergence characteristics for thin rectangular plates ($B/L = 3.0$): central deflection normalised with respect to exact thin plate theory [23].

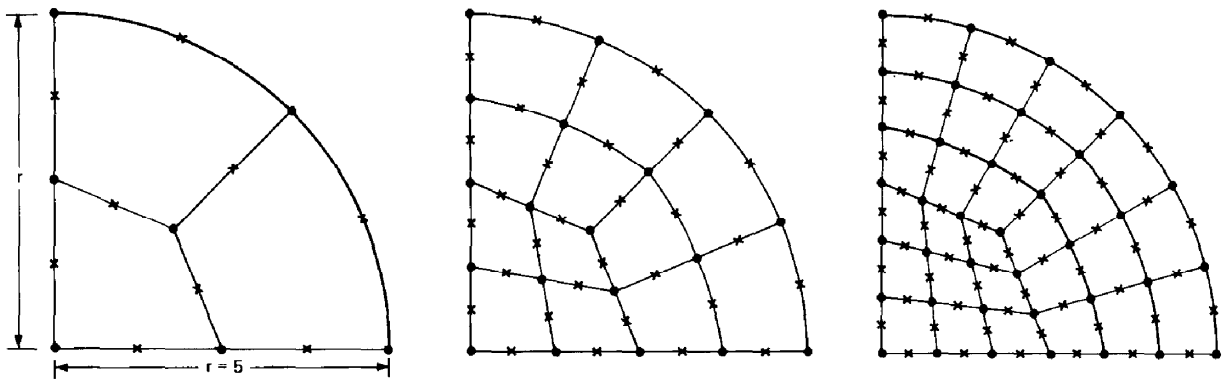

Fig. 9. Mesh divisions for circular plates. · Corner nodes; × mid-sides (only presented for element S8).

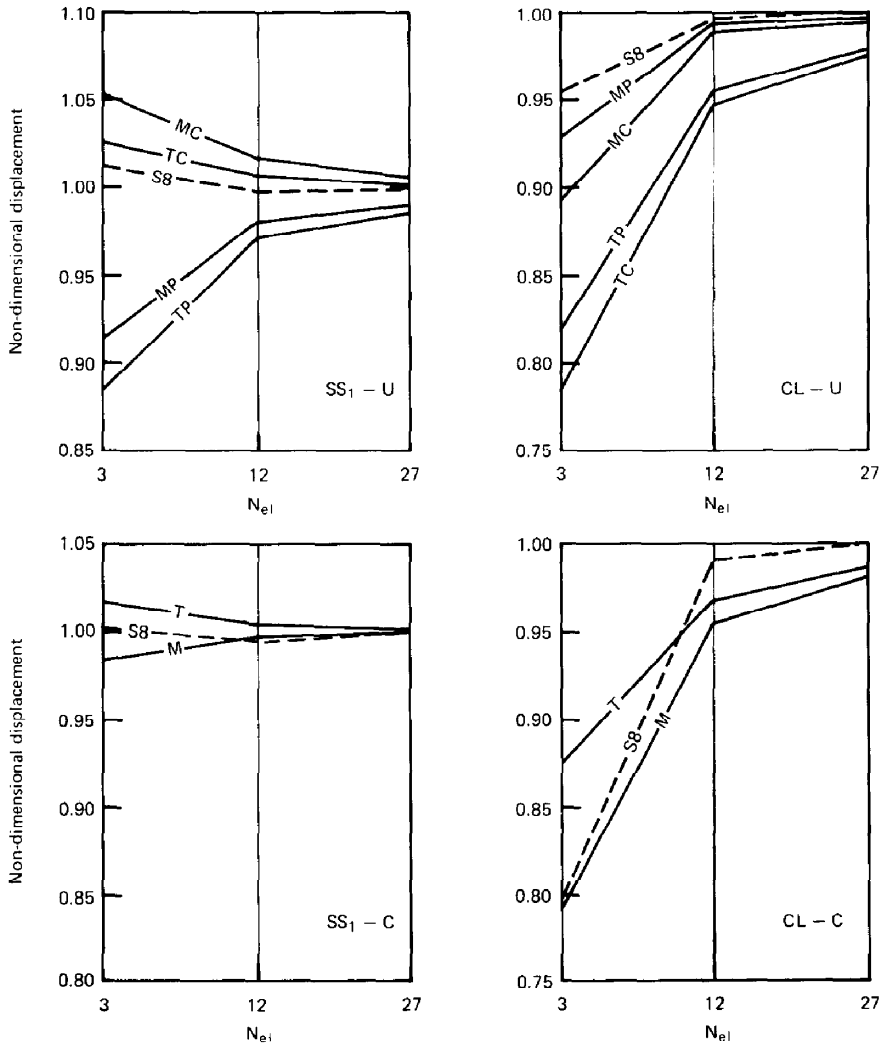

Fig. 10. Convergence characteristics for thin circular plates: central deflection normalised with respect to exact thin plate theory [23].

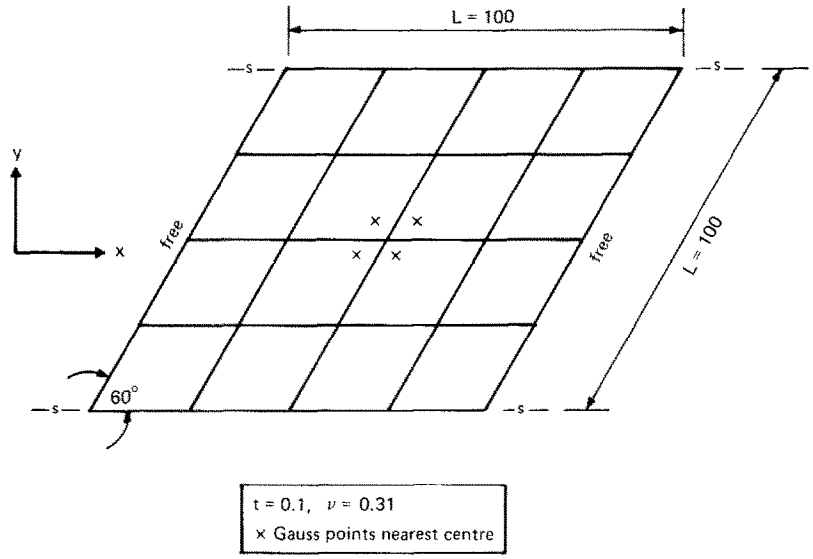

Fig. 11. Skew plate simply supported on two sides: Geometry and 4 × 4 mesh.

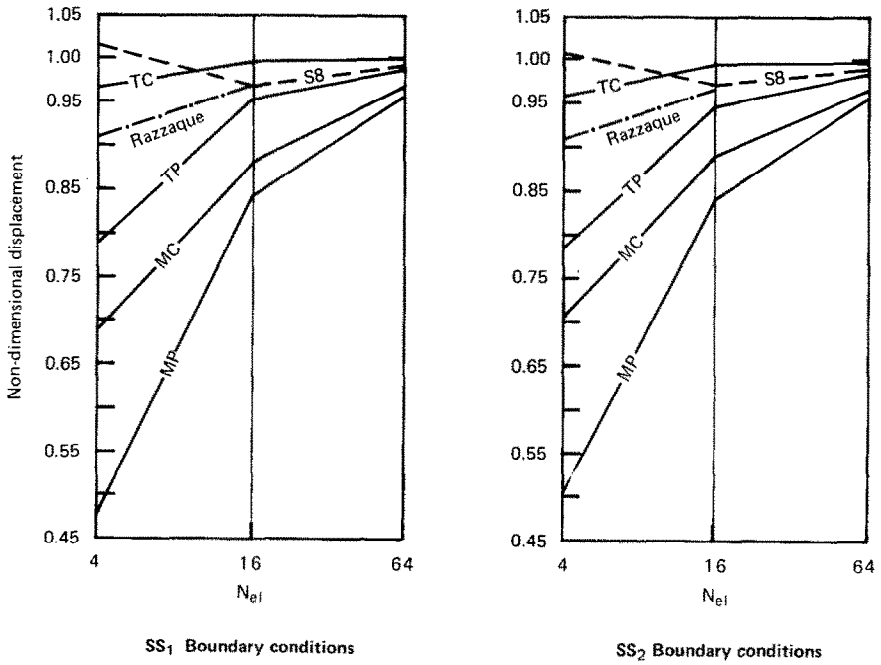

Fig. 12. Convergence characteristics for Razzaque's skew plate: central deflection normalised with respect to 16 × 16 finite difference solution [26].

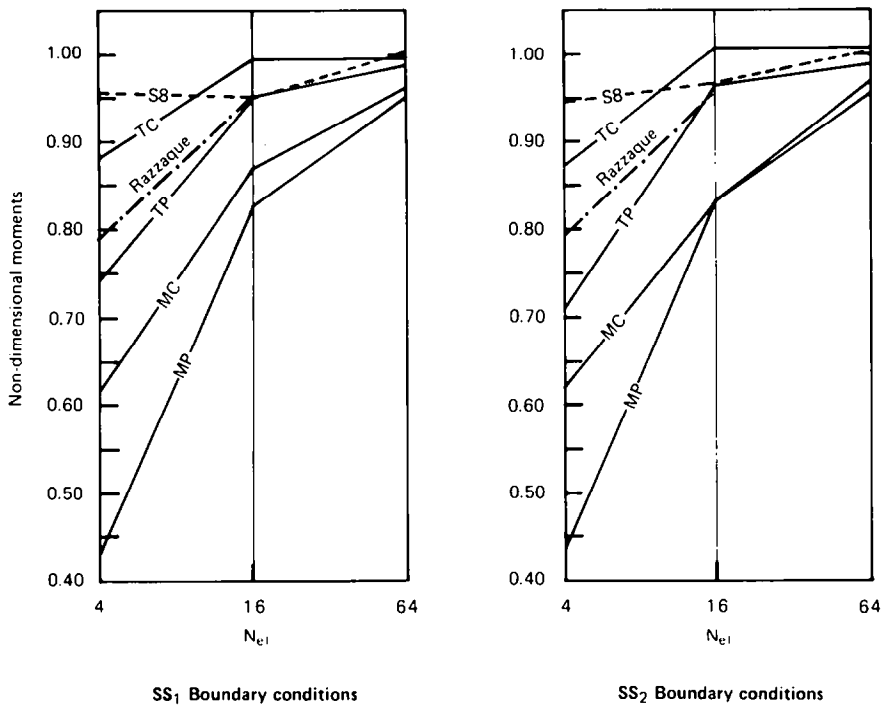

Fig. 13. Convergence characteristics for Razzaque's skew plate: average moment M_y from Gauss points, nearest centre, normalised with respect to 16 × 16 finite difference solution at centre [26].

but, since the elements are triangles, the division by two is appropriate in order to make a valid comparison with parallelogram elements. The bending moments, shown in Fig. 13 for elements M, T and S8, were found by averaging those from the two-point Gauss stations nearest to the centre (Fig. 11) while Razzaque's results were found using interpolation from the element mid-side values [26].

It appears from Figs. 12 and 13 that, of the parallelogram elements, S8 gives the best results (on an element-for-element basis, which is unfair on the four-noded elements), although the

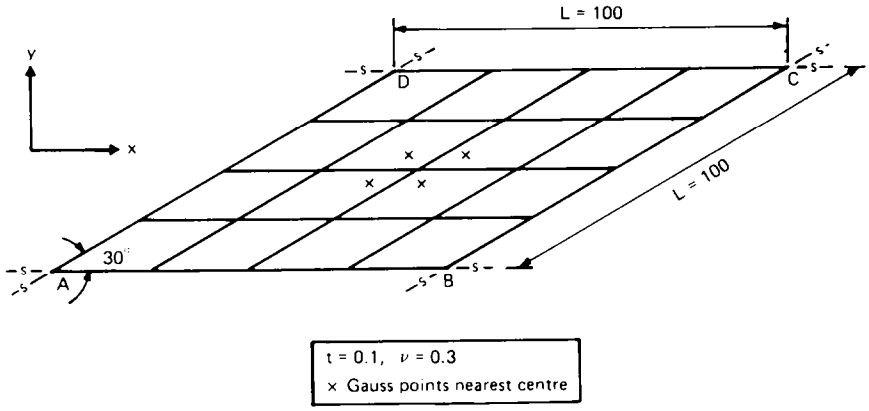

Fig. 14. Morley's acute skew plate: geometry and 4 × 4 mesh.

thin-plate element T gives very comparable solutions. The other results, involving four-noded elements, are much less satisfactory. The solutions, that were obtained with the thin-plate element using the consistent load vector (TC) and the SS_1 boundary conditions, were found to coincide with those given by Lyons [1] for his ISOFLEX 4 element.

(e) *Morley's acute skew plate.* Morley [28] used polar co-ordinates and a least squares solution procedure to analyse an acute skew plate (Fig. 14), subjected to a uniformly distributed load. This problem poses severe difficulties for numerical methods, since there is a singularity in the bending moments at the obtuse corner. Despite these difficulties, Morley's solution is effectively exact in relation to thin plate theory.

Using the standard finite element displacement variables, two types of boundary condition can be applied to this problem (see Fig. 14):

(I) SS_1 on all sides.

(II) SS_1 on sides AD and BC and SS_2 on sides AB and CD.

Both boundary conditions have been applied and the results are plotted in Figs. 15 and 16.

The present thin-plate element gives excellent convergence characteristics, which are far superior to those exhibited by the two Mindlin elements. (The results for the eight-noded S8 element are particularly bad.) The 'TC Boundary Condition I' solutions coincide with those given by Lyons [1] for his ISOFLEX 4 element. Following the general trend of the previous examples, the consistent load vector leads to more flexible solutions than those obtained with the lumped point loads. For the thin-plate element, the lumped point loads unusually give the better solutions, although those obtained with the consistent load vector are also very good. For Hughes and Tezdulyar's Mindlin element, the better, more flexible, solutions are obtained with the consistent load vector.

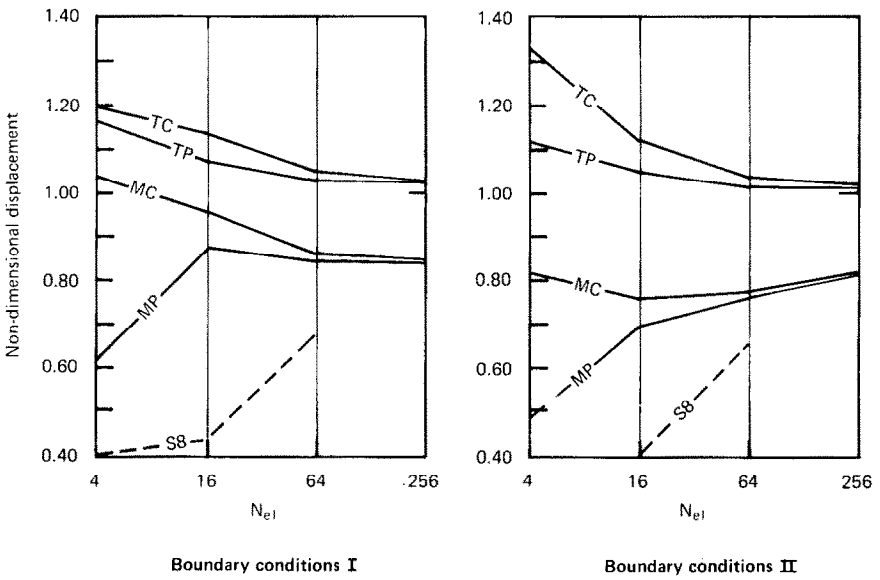

Fig. 15. Convergence characteristics for Morley's skew plate: central deflection normalised with respect to 'exact' thin plate solution [28].

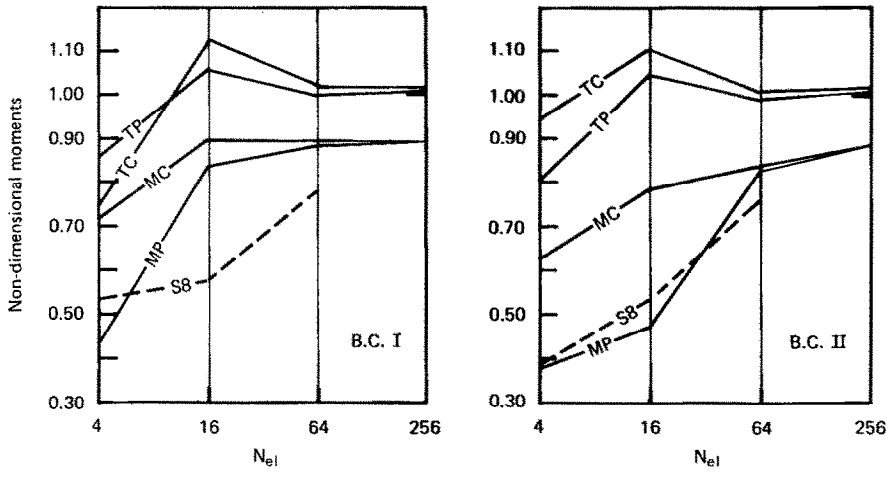

(a) Major principal moments

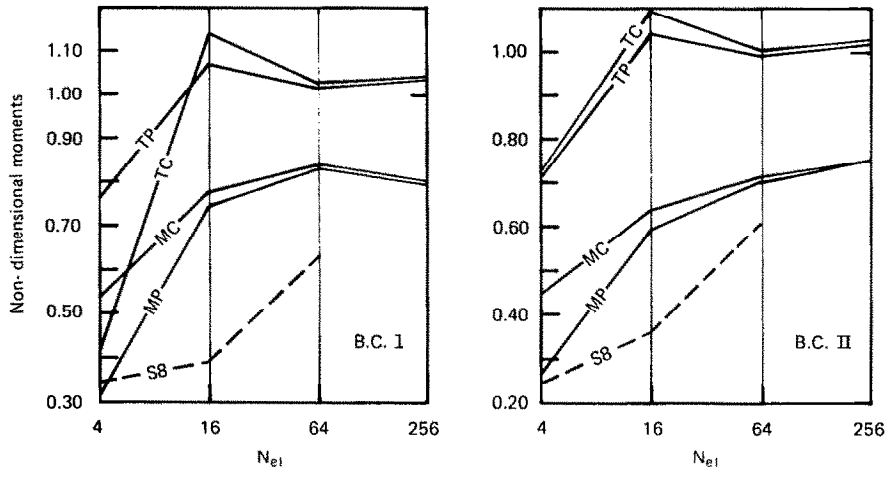

(b) Minor principal moments

Fig. 16. Convergence characteristics for Morley's skew plate: average principal moments from Gauss points, nearest centre, normalised with respect to exact, central thin plate moments [28].

7. Conclusions

A four-noded thin-plate bending element has been derived using shear constraints. Numerical experiments have indicated that, for rectangles and parallelograms, the element gives identical results to Lyons' ISOFLEX 4 element [1]. The experiments have also shown that, for such geometries, this element gives a superior performance to both Hughes and Tezduyar's four-noded Mindlin element [13] and the eight-noded serendipity element, using two-point Gaussian integration [9, 10]. This superiority is most apparent in relation to the

skew plates that have been analysed. Inevitably, these conclusions only relate to thin-plates since, unlike the Mindlin elements, the present element cannot account for shear deformation.

Lyons has not given any examples, other than the patch test, which involve his four-noded element in the context of a general quadrilateral. Hence, it has not been possible to ascertain whether, or not, the present element always gives an identical performance. General quadrilaterals have, however, been used for the present element in relation to the analysis of a circular plate subject to various loads and boundary conditions. The solutions, although inferior to those given by Hughes and Tezduyar's four-noded Mindlin element, for the clamped plate subject to a uniformly distributed load, were nonetheless very adequate, considering the idealisation involves a straight-sided perimeter. Both the present element and Lyons' predecessor pass the patch test for a general quadrilateral.

The numerical experiments indicate that a consistent load vector should be used for the application of uniformly distributed loads to the present (or Lyons') element. They also indicate that the application of such a load vector to Hughes and Tezduyar's four-noded Mindlin element leads to more flexible solutions than those obtained with a lumped point load vector (as used by Hughes and Tezduyar). For this element, these more flexible solutions were generally worse than those obtained with the lumped point load vector, when rectangular plates were analysed, but were better for skew plates.

Although the performance of the present element appears identical to that of Lyons' element for rectangles and parallelograms, the derivation is, in some important respects, different. In particular, the present constraints ensure that the tangential shear strain is 'effectively zero' along both the sides (as Lyons) and the two 'centre-lines' (different from Lyons). Also, these constraints are derived in explicit algebraic form so that they can be easily implemented. Fortran subroutines are provided for the computation of the constrained curvature–nodal displacement matrix, which is the main ingredient for the element stiffness matrix.

Appendix A. The hierarchical shape functions and derivatives

In relation to Fig. 2(b), the original shape functions and derivatives are given by

$$H_i = \begin{cases} \frac{1}{4}(1+\xi_i\xi)(1+\eta_i\eta) & \text{for } i = 1\text{–}4\,, \\ \frac{1}{2}(1-\eta_i^2\xi^2-\xi_i^2\eta^2)(1+\xi_i\xi+\eta_i\eta) & \text{for } i = 5\text{–}8\,, \\ (1-\xi^2)(1-\eta^2) & \text{for } i = 9\,, \end{cases}$$

$$\begin{aligned} H_{\xi i} &= \tfrac{1}{4}\xi_i(1+\eta_i\eta) \\ H_{\eta i} &= \tfrac{1}{4}\eta_i(1+\xi_i\xi) \end{aligned} \quad \text{for } i = 1\text{–}4\,,$$

$$\begin{aligned} H_{\xi i} &= -\eta_i\xi(\eta_i+\eta)+\tfrac{1}{2}\xi_i(1-\eta^2) \\ H_{\eta i} &= -\xi_i\eta(\xi_i+\xi)+\tfrac{1}{2}\eta_i(1-\xi^2) \end{aligned} \quad \text{for } i = 5\text{–}8\,,$$

$$\begin{aligned} H_{\xi 9} &= -2\xi(1-\eta^2)\,, \\ H_{\eta 9} &= -2\eta(1-\xi^2)\,. \end{aligned}$$

Appendix B. Two subroutines for the generation of the constrained curvature–nodal displacement matrix

It is assumed that the unit 'side' direction vectors e_1–e_6 (E(6,2)) have been formed in conjunction with the side lengths h_1–h_6 (HT(6)). The indexing is such that $e_3(1)$ = E(3,1), for example. The inverse Jacobian J^{-1} (AJI (2,2)) at the relevant point (ξ, η) is also required as are the shape function derivatives (see Appendix A), $H_{\xi i}$, i = 1–9 in (P(1,I), I = 1–9) and $H_{\eta i}$, i = 1–9 in (P(2,I), I = 1–9).

The subroutines are not designed for optimal efficiency in computing terms, but rather, to relate clearly to the theoretical developments in the paper. The main subroutine BMATRIX forms the constrained curvature–nodal displacement matrix, B_c, in (BC(3,12)), where the final twelve nodal displacements are stored as indicated in equations (49) and (39).

```
      SUBROUTINE BMATRIX(BC,E,HT,P,AJI)
C     CALCULATES CONSTRAINED 'CURVATURE'-
C     DISPLACEMENT MATRIX BC(3,12)-EQN.(27)
C     GIVEN 'SIDE' DIRN. VECTORS,E,'SIDE' LENGTHS,HT,
C     SHAPE FN. DERIVATIVES P AND INVERSE
C     JACOBIAN AJI(2,2)
      DIMENSION BC(3,12),E(6,2),HT(6),P(2,9),AJI(2,2)
      DIMENSION B(3,27),XI(9),ETA(9),C9(2,24)
      DIMENSION IPLUS(4), CA(3,3),CB(3,3)
      DATA XI/1.0,-1.0,-1.0,1.0,0.0,-1.0,0.0,1.0,0.0/
      DATA ETA/1.0,1.0,-1.0,-1.0,1.0,0.0,-1.0,0.0,0.0/
      DATA IPLUS/2,3,4,1/
C
      DO 1 I = 1,3
      DO 1 J = 1,27
    1 B(I,J) = 0.
      DO 2 I = 1,9
      I3 = 3*(I - 1)
      TX = AJI(1,1)*P(1,I) + AJI(1,2)*P(2,I)
      TY = AJI(2,1)*P(1,I) + AJI(2,2)*P(2,I)
      B(1,I3 + 2) = TX
      B(2,I3 + 3) = TY
      B(3,I3 + 2) = TY
      B(3,I3 + 3) = TX
    2 CONTINUE
C     ABOVE FORMS UNCONSTRAINED B MATRIX(EQN.27)
      CALL BUBCON(C9,E,HT,XI,ETA)
C     ABOVE GETS BUBBLE-FN. SLOPE CONSTRAINT MAT.C9
      DO 3 I = 1,3
      DO 4 J = 1,24
      DO 5 K = 1,2
    5 B(I,J) = B(I,J) + B(I,K + 25)*C9(K,J)
    4 CONTINUE
    3 CONTINUE
C     ABOVE 'DISPERSES' BUBBLE-FN. TERMS.
      DO 6 I = 1,4
      CA(1,1) = 0.
```

```
      CA(1,2) = −0.125*HT(I)*E(I,1)
      CA(1,3) = −0.125*HT(I)*E(I,2)
      CA(2,1) = 1.5*E(I,1)/HT(I)
      CA(2,2) = −0.75*E(I,1)*E(I,1)
      CA(2,3) = −0.75*E(I,1)*E(I,2)
      CA(3,1) = 1.5*E(I,2)/HT(I)
      CA(3,2) = CA(2,3)
      CA(3,3) = −0.75*E(I,2)*E(I,2)
      DO 7 J = 2,3
      DO 8 K = 2,3
    8 CB(J,K) = CA(J,K)
      CB(1,J) = −CA(1,J)
      CB(J,1) = −CA(J,1)
    7 CONTINUE
C     FOR ABOVE SEE EQN. (40)
      I3 = 3*(I − 1)
      IP = IPLUS(I)
      IP3 = 3*(IP − 1)
      IPM = 3*(I + 3)
      DO 9 JJ = 1,3
      DO 10 J = 1,3
      II = I3 + J
      IPJ = IP3 + J
      DO 11 K = 1,3
      IK = IPM + K
      B(JJ,II) = B(JJ,II) + B(JJ,IK)*CA(K,J)
   11 B(JJ,IPJ) = B(JJ,IPJ) + B(JJ,IK)*CB(K,J)
C     ABOVE APLLIES MID-SIDE CONST. OF EQ. (38)
   10 CONTINUE
    9 CONTINUE
    6 CONTINUE
      DO 12 I = 1,3
      DO 12 J = 1,12
   12 BC(I,J) = B(I,J)
      RETURN
      END


      SUBROUTINE BUBCON(C9,E,HT,XI,ETA)
C     CALCULATES C9(2,24)–THE CONSTRAINT MATRIX
C     CONNECTING DEL THETA 9 AND THE OTHER VARIABLES(EQN.(48))
C     GIVEN 'SIDE' DIRN. VECTORS,E,'SIDE' LENGTHS HT
C     AND NON–D CO–ORDS. OF NODES,XI AND ETA(SEE S/R BMATRIX)
      DIMENSION C9(2,24),E(6,2),HT(6),XI(9),ETA(9)
      DIMENSION N5(2),N6(2),N5E(2,2),N6E(2,2)
      REAL N5,N6,N5E,N6E
C
      PHI = E(5,1)*E(6,2)–E(5,2)*E(6,1)
      N5(1) = −E(5,2)/PHI
      N5(2) = E(5,1)/PHI
      N6(1) = −E(6,2)/PHI
      N6(2) = E(6,1)/PHI
C     ABOVE RELATES TO EQS, (45) AND (46)
```

```
      DO 1 I = 1,2
      DO 1 J = 1,24
    1 C9(I,J) = 0.
      DO 2 I = 1,2
      DO 2 J = 1,2
      N5E(I,J) = N5(I)*E(6,J)/3.
      N6E(I,J) = N6(I)*E(5,J)/3.
    2 CONTINUE
      DO 3 I = 1,4
      IP = I + 4
      IP = 3*(I - 1)
      IP3 = 3*(IP - 1)
      XP2 = 0.75*XI(IP)*XI(IP)
      EP2 = 0.75*ETA(IP)*ETA(IP)
      C9(1,I3 + 2) = -3./8.
      C9(2,I3 + 3) = -3./8.
C     ABOVE THETA TERMS
      C9(1,IP3 + 2) = -0.75
      C9(2,IP3 + 3) = -0.75
C     ABOVE SOME OF DEL THETA TERMS
      DO 4 JJ = 1,2
      C9(JJ,I3 + 1) = -0.75*((ETA(I)*N5(JJ)/HT(6))-
    1 (XI(I)*N6(JJ)/HT(5)))
C     ABOVE W TERMS
      C9(JJ,IP3 + 1) = -1.5*((ETA(IP)*N5(JJ)/HT(6))-
    1 (XI(IP)*N6(JJ)/HT(5)))
C     ABOVE DEL W TERMS
      DO 5 J = 1,2
      II = IP3 + J + 1
      C9(JJ,II) = C9(JJ,II) + XP2*N5E(JJ,J)-EP2*N6E(JJ,J)
C     ABOVE REST OF DEL THETA TERMS
    5 CONTINUE
    4 CONTINUE
    3 CONTINUE
      RETURN
      END
```

References

[1] L.P.R. Lyons, A general finite element system with special reference to the analysis of cellular structures. Ph.D. Thesis, Imperial College of Science and Technology, London, 1977.

[2] G. Dhatt, Numerical analysis of thin shells by curved triangular elements based on discrete Kirchhoff hypothesis, Proc. ASCE Symp. Application of FEM in Civil Engineering, Vanderbilt University, Nashville, TN (1979) 13–14.

[3] J.-L. Batoz, K.-J. Bathe and L.-W. Ho, A study of three-node plate bending elements, Internat J. Numer. Meths. Engrg. 15 (1980) 1771–1812.

[4] B.M. Irons, The semi-loof shell element, in: D.G. Ashwell and R.H. Gallagher, eds., Finite Elements for Thin Shells and Curved Membranes (Wiley, New York, 1976) 197–222.

[5] B.M. Irons and S. Ahmad, Techniques of Finite Elements (Ellis Horwood, Chichester, 1980).

[6] J.T. Baldwin, A. Razzaque and B.M. Irons, Shape function subroutine for an isoparametric thin plate element, Internat. J. Numer. Meths. Engrg. 7 (1973) 431–440.

[7] O.C. Zienkiewicz, The Finite Element Method (McGraw-Hill, New York, 1977).
[8] R.D. Mindlin, Influence of rotary inertia and shear on flexural motions of isotropic elastic plates, J. Appl. Mech. 18 (1951) 31–38.
[9] O.C. Zienkiewicz, R.L. Taylor and J.M. Too, Reduced integration techniques in general analysis of plates and shells, Internat. J. Numer. Meths. Engrg. 3 (1971) 275–290.
[10] S.E. Pawsey and R.W. Clough, Improved numerical integration of thick shell finite elements, Internat. J. Numer. Meths. Engrg. 3 (1971) 545–586.
[11] B.M. Irons and A. Razzaque, Shape function formulations for elements other than displacement models, in: C. Brebbia et al., eds., Variational Methods in Engineering (Southampton University Press, Southampton, 1973) 4/59–4/72.
[12] A. Tessler and S.B. Dong, On a hierarchy of conforming Timoshenko beam elements, Comput. & Structures 8 (1978) 175–183.
[13] T.J.R. Hughes and T.E. Tezduyar, Finite elements based upon Mindlin plate theory, with particular reference to the four-node bi-linear isoparametric element, J. Appl. Mech. (1981) 587–596.
[14] R.H. MacNeal, A simple quadrilatral shell element, Comput. & Structures 8 (1978) 175–183.
[15] J. Robinson and G.W. Haggenmacher, Lora—an accurate four node stress plate bending element, Internat. J. Numer. Meths. Engrg. 14 (1979) 296–306.
[16] T.J.R. Hughes, M. Cohen and M. Haroun, Reduced and selective integration techniques in the finite element analysis of plates, Nuclear Engrg. Design 46 (1978) 203–222.
[17] E.D.L. Pugh, E. Hinton and O.C. Zienkiewicz, A study of quadrilateral plate bending elements with reduced integration, Internat. J. Numer. Meths. Engrg. 12 (1978) 1059–1079.
[18] T. Belytschko, C.S. Tsay and W.K. Liu, A stabilisation matrix for the bilinear Mindlin plate element, Comput. Meths. Appl. Mech. Engrg. 29 (1981) 313–327.
[19] T.J.R. Hughes and M. Cohen, The 'heterosis' finite element for plate bending, Comput. & Structures 9 (1978) 445–450.
[20] M.A. Crisfield, A quadratic Mindlin element using shear constraints, Comput & Structures, to appear.
[21] B. Fraeijs de Veubeke, Displacement and equilibrium models in the finite element method, in: O.C. Zienkiewicz and G.S. Holister, eds., Stress Analysis (Wiley, New York, 1965) 145–197.
[22] S.P. Timoshenko, On the correction for shear of the differential equation for transverse vibration of prismatic bars, Philos. Mag. 41 (1921) 744–746.
[23] S. Timoshenko and S. Woinowsky-Krieger, Theory of Plates and Shells (McGraw-Hill, London, 1959).
[24] P. Djahani, Elastic-plastic analysis of discretely stiffened plates, Ph.D. Thesis, Imperial College of Science and Technology, London, 1977.
[25] E. Hinton, F.C. Scott and R.E. Ricketts, Local least squares stress smoothing for parabolic isoparametric elements, Internat. J. Numer. Meths. Engrg. 9 (1975) 235–238.
[26] A. Razzaque, Program for triangular bending elements with derivative smoothing, Internat. J. Numer. Meths. Engrg. 6 (1973) 333–343.
[27] D.J. Allman, Triangular finite elements for plate bending with constant and linearly varying bending moments, IUTAM Symp. High-speed Comp. Elastic Struct. Liege, 1970.
[28] L.S.D. Morley, Skew Plates and Structures (Pergamon, Oxford, 1963).